

000

001

002

003

004

005

006

007

008

009

010

011

012

013

014

015

016

017

018

019

020

021

022

023

024

025

026

027

028

029

030

031

032

033

034

035

036

037

038

EQUIBIND: Geometric Deep Learning for Drug Binding Structure Prediction

Anonymous Authors¹

Abstract

Predicting how a drug-like molecule binds to a specific protein target is a core problem in drug discovery. An extremely fast computational binding method would enable key applications such as fast virtual screening or drug engineering. Existing methods are computationally expensive as they rely on heavy candidate sampling coupled with scoring, ranking, and fine-tuning steps. We challenge this paradigm with EQUIBIND, an SE(3)-equivariant geometric deep learning model performing direct-shot prediction of both i) the receptor binding location (blind docking) and ii) the ligand's bound pose and orientation. EquiBind achieves significant speed-ups and better quality compared to traditional and recent baselines. Further, we show extra improvements when coupling it with existing fine-tuning techniques at the cost of increased running time. Finally, we propose a novel and fast fine-tuning model that adjusts torsion angles of a ligand's rotatable bonds based on closed-form global minima of the von Mises angular distance to a given input atomic point cloud, avoiding previous expensive differential evolution strategies for energy minimization.

1. Introduction

Drug discovery is an expensive process, e.g., a single drug costs around 1 billion dollars and takes 10 years of development and testing before potentially being FDA approved. Moreover, this process can fail at any point, e.g., due to unforeseen side effects or experimental disproof of the promised therapeutic efficacy. Worse, there are 10^{60} possible drug-like molecules (Reymond & Awale, 2012), going far beyond current experimental capabilities.

Accurate computational methods, e.g., deep learning (DL)

¹Anonymous Institution, Anonymous City, Anonymous Region, Anonymous Country. Correspondence to: Anonymous Author <anon.email@domain.com>.

Preliminary work. Under review by the International Conference on Machine Learning (ICML). Do not distribute.

based, can drastically reduce the molecular search space, but need to be extremely fast to scan the vast biological and chemical spaces for both desired and unexpected effects. For instance, a novel drug that inactivates an important cancer protein might negatively inhibit other essential proteins in the human body, potentially resulting in life-threatening side effects. Given that the human proteome contains up to 100,000 protein types, the current hope is to scan for these interactions in a computational manner before bringing a few promising candidates to *in vitro* and *in vivo* testing.

A core problem in drug discovery is understanding how drug-like molecules (ligands) interact and form complexes with target proteins (receptors) – *drug binding* – which is a prerequisite for virtual screening. This is a difficult problem with different facets and constraints: binding kinetics, conformational changes (internal molecular flexibility), and chemical and geometrical atomic interaction types are part of the domain knowledge describing ligand-protein binding mechanisms (Du et al., 2016). For instance, classical models for molecular complex formation are "lock-and-key", "induced fit", and "conformational selection", while hydrophobic, hydrogen-bonding, and π -stacking are the most frequent atomic binding interactions, but other types often occur during binding (de Freitas & Schapira, 2017).

Current *in silico* approaches for (3D) structural drug binding achieve high quality at a significant computational cost, e.g., the GNINA method (McNutt et al., 2021) takes on average 57 minutes for a single ligand-receptor pair, while the popular commercial software Glide (Halgren et al., 2004) is up to 5 times slower. This is caused by the common strategy employed by all previous binding methods: first, a large set of candidate complexes (e.g., millions) is generated via thorough sampling of possible binding locations and poses (Hassan et al., 2017); then, scoring and ranking steps are used to retrieve the most promising instances; finally, an energy-based fine-tuning method is employed to best fit the ligand in the respective pocket locations.

Here, we introduce EQUIBIND, a novel geometric & graph deep learning model for structural drug binding – Figure 1. Inspired by Ganea et al. (2021a), we exploit graph matching networks (GMN) (Li et al., 2019) and E(3)-equivariant graph neural networks (E(3)-GNN) (Satorras et al., 2021) to perform a direct prediction of the ligand-receptor com-

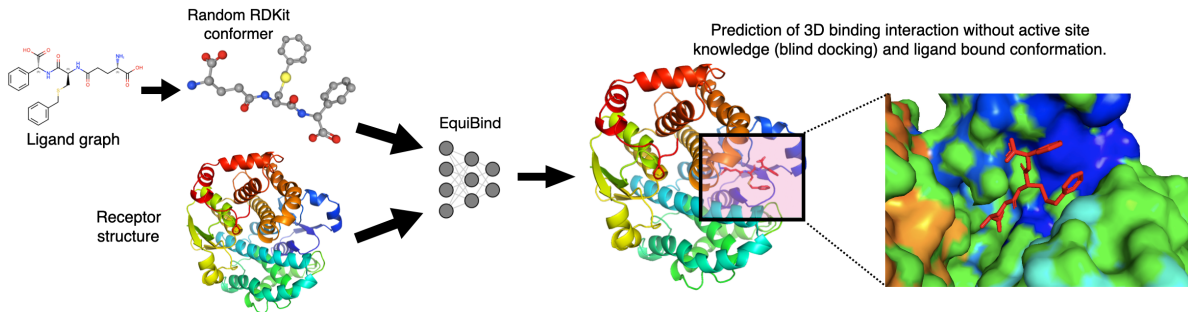


Figure 1. High-level overview of the structural drug binding problem tackled by EQUIBIND.

plex structure without relying on heavy sampling as prior work, thus achieving **significant inference time speed-ups**. Moreover, since 3D structural data suffers from scarcity (e.g., only around 19K experimental complexes are publicly available in the PDBbind database), it is crucial to inject the right physical, chemical, or biological *inductive biases* into DL models to avoid learning these priors from insufficient amounts of data and to create trustable models. Towards this goal, EQUIBIND:

- guarantees independence to the initial 3D placements and orientations of the two molecules, i.e., the exact same complex is always predicted for the same input unbound structures,
- incorporates an efficient mechanism for biologically plausible ligand flexibility by only altering torsion angles of rotatable bonds while keeping local structures (bond angles and lengths) fixed,
- utilizes a non-intersection loss to prevent steric clashes or unrealistic van der Waals interactions.

We focus on the *blind docking* scenario, i.e., zero knowledge of the protein's binding site or pocket. However, our method can easily be adapted to situations where the approximate binding location is known. Similar to (Zhang et al., 2020), we argue that errors in the ground truth binding pocket conformation heavily affect traditional docking methods that are conditioned on the receptor active site (Lang et al., 2009; Trott & Olson, 2010). In practice, the ground truth 3D locations of the binding atoms might be low-resolution, might not be known at all (e.g., for novel antigens), or we might be interested in discovering new druggable locations on a protein's surface that were previously thought to be undruggable (e.g. exploring allosteric binding locations rather than orthosteric sites).

Empirically, we investigate two settings: re-docking (i.e., taking the bound ligand structure out of a complex and asking the model to dock it) and flexible self-docking (i.e., ligands have no bound structure knowledge prior to docking). We assume a rigid receptor, but we model ligand flexibility by first predicting an atomic point cloud of the deformed molecule and then employing a fast algorithm to extract in-

ternal changes of rotatable bonds' torsion angles that would match the point cloud as well as possible. Instead of minimizing the root-mean-square deviation (RMSD) using expensive optimization strategies (e.g., differential evolution approaches (Méndez-Lucio et al., 2021)), we maximize the log-likelihood of a von Mises distribution that fits the torsion angles, proving closed-form expressions of the global optimum. Experimentally, we show improved quality in various metrics over popular and recent state-of-the-art baselines at a fraction of the running time. Finally, we show the power of combining EquiBind with existing energy-based methods to realize a hybrid DL approach. Indeed, we believe the future of computational drug discovery will follow the paradigm demonstrated here.

2. Related Work

We now dive into various research directions relevant for structural and DL-based drug binding.

Protein and molecular structure prediction. Obtaining experimental 3D structural data of molecules and proteins is a highly expensive process. However, very recent DL models have produced a breakthrough in computational protein folding (Jumper et al., 2021b; Baek et al., 2021) and fast generation of small molecule low-energy conformation ensembles (Ganea et al., 2021b; Luo et al., 2021; Xu et al., 2020; Shi et al., 2021). These methods aim to accelerate the discovery of new structures and complement experimental data in various applications such as drug discovery.

Protein representations (for DL-based molecular interactions). To be useful for predicting molecular interactions, proteins must be modeled in specific ways to account for different views: backbone & side-chains, protein surface, atomic point cloud, or amino-acid sequence. Somnath et al. (2021) create a hierarchical representation of proteins and prove its utility in binding and function prediction. Gainza et al. (2020); Sverrisson et al. (2021) leverage geometric deep learning and mesh convolutional neural networks (CNN) to embed protein surface patches into fingerprints and allow for fast scanning and binding site identification, removing the need for handcrafted or

expensive pre-computed features. However, these methods do not perform the full structural blind docking task that involves prediction of the binding site, of the orientations and placements of the two molecular structures, and of the internal conformational deformations during binding. Various other protein representations have been proposed for (graph) DL methods for individual structure prediction (Jing et al., 2020), protein-protein interactions (Dai & Bailey-Kellogg, 2021; Eismann et al., 2020; Townshend et al., 2019), or protein function prediction (Gligorijević et al., 2021).

Druggable binding site identification. Traditional computational methods for scanning proteins for their most "druggable" areas have leveraged various views such as utilizing the protein's 3D structure or/and residue sequence, extracting geometric features, building large template libraries, or relying on energy-based models (Macari et al., 2019). Recently, DL changed this paradigm, e.g., using 3D CNNs (Aggarwal et al., 2021; Jiménez et al., 2017; Torng & Altman, 2019b) or sequence models (Sankararaman et al., 2010).

Popular and more recent drug binding models. Representative docking software for drug-like molecules are AutoDock Vina (Trott & Olson, 2010) and its various extensions for improving speed (Trott & Olson, 2010), scoring (Koes et al., 2013) or for blind docking (Hassan et al., 2017). As mentioned in Section 1, these methods employ a multi-stage strategy based on heavy candidate sampling, scoring, ranking, and fine-tuning. Various subsequent methods aimed to improve some parts of this pipeline (Zhang et al., 2020; Mohammad et al., 2021; McNutt et al., 2021; Francoeur et al., 2020), with a special emphasis on the scoring function – see below.

GNNs and CNNs for binding scoring functions and binding affinity prediction. Deep learning on 3D voxel images (via 3D CNNs) or interaction graphs (via GNNs) have improved the traditional hand-designed scoring function used in AutoDock Vina, enabling better fine-tuning of predicted docked poses, as well as direct binding affinity prediction from the 3D complex (McNutt et al., 2021; Francoeur et al., 2020; Ragoza et al., 2017; Wallach et al., 2015; Lim et al., 2019; Morrone et al., 2020; Jiang et al., 2021; Shen et al., 2021; Jastrzebski et al., 2020; Bao et al., 2021; Torng & Altman, 2019a; Li et al., 2021). However, some methods (Karimi et al., 2019; Gao et al., 2018) have found that using the protein sequence and the drug SMILES string already provide competitive predictions for binding affinity without the need of 3D structural data.

Closer to our approach, Méndez-Lucio et al. (2021) has shown that optimizing the ligand's global 3D position and orientation and the torsion angles of rotatable bonds to minimize a GNN based scoring function improves fine-tuning of the ligand into the active site and its predicted bound pose. However, they employ differential evolution for this

optimization, and we find it to be slow in practice (e.g., 29 sec for a 5-rotatable bond molecule and 50 min for a 44-rotatable bond molecule). Instead, our proposed EQUIBIND optimizes in closed form a ligand's torsion angles to match a predicted atomic point cloud in less than 1 sec.

Applications of drug binding methods. Computational docking methods are employed for various facets of drug discovery, e.g., fast virtual screening (Gniewek et al., 2021; Jastrzebski et al., 2020) or de novo binder generation (Masa- suda et al., 2020; Imrie et al., 2021; Drotár et al., 2021).

Deep learning for protein-protein docking. A related problem is *protein-protein docking* in which recent methods have performed direct prediction of the complex structure from the two concatenated input sequences using evolutionary information (Evans et al., 2021), or have leveraged geometric deep learning to model rigid body docking (Ganea et al., 2021a) or side-chains structures (Jindal et al., 2021).

Incorporating Euclidean symmetries into GNNs. Injecting Euclidean 3D transformations into geometric DL models has become possible using equivariant message passing layers (Cohen & Welling, 2016; Thomas et al., 2018; Fuchs et al., 2020; Satorras et al., 2021; Brandstetter et al., 2021; Batzner et al., 2021). Our method follows Ganea et al. (2021a) to incorporate SE(3) pairwise equivariance into message passing neural networks for the drug binding problem. However, different from this method, we go beyond rigid docking and model ligand conformational flexibility.

3. EQUIBIND Model

We describe our EQUIBIND model, highlighted in Figure 1 and detailed in Figure 2. It takes as input a ligand molecular graph with a random associated unbound 3D conformer (e.g., generated using RDKit/ETKDG (Riniker & Landrum, 2015)), as well as a receptor-bound structure. As previously noted, we only model ligand flexibility in this work, assuming a rigid protein conformation.

K-NN graph representations. We represent both input molecules as spatial k-nearest neighbor (k-NN) graphs. The ligand graph $\mathcal{G} = (\mathcal{V}, \mathcal{E})$ uses atoms as nodes with their respective 3D coordinates from the unbound conformer denoted as $\mathbf{X} \in \mathbb{R}^{3 \times n}$, and initial features $\mathbf{F} \in \mathbb{R}^{d \times n}$ (e.g., atom type). Edges include all atom pairs within a distance cutoff of 4 Å. The receptor graph $\mathcal{G}' = (\mathcal{V}', \mathcal{E}')$ has residues as nodes and their 3D coordinates $\mathbf{X}' \in \mathbb{R}^{3 \times m}$ are given by the α -carbon locations. We also include the same node features as (Ganea et al., 2021a), denoted here as $\mathbf{F}' \in \mathbb{R}^{d' \times m}$. Each node is connected in the graph to the closest 10 other nodes at less than 30 Å distance.

Independent E(3)-equivariant transformations. Similar to (Ganea et al., 2021a), an important geometric induc-

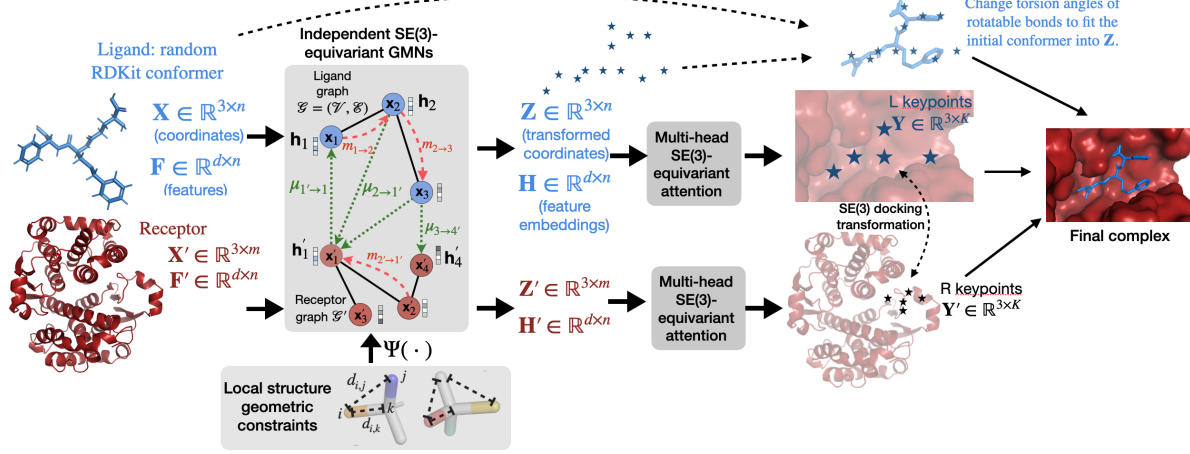


Figure 2. EQUIBIND model architecture.

tive bias is to predict the same binding complex no matter how the initial molecules are positioned and oriented in space. This is especially needed for data-scarce problems such as structural drug binding. Towards this goal, we use *Independent E(3)-Equivariant Graph Matching Network* (IEGMN) (Ganea et al., 2021a) which combines Graph Matching Networks (Li et al., 2019) and E(3)-Equivariant Graph Neural Networks (Satorras et al., 2021). This architecture jointly transforms both features and 3D coordinates to perform *intra* and *inter* neural graph message passing. Formally, $IEGMN(\mathbf{X}, \mathbf{F}, \mathbf{X}', \mathbf{F}') = \mathbf{Z} \in \mathbb{R}^{3 \times n}, \mathbf{H} \in \mathbb{R}^{d \times n}, \mathbf{Z}' \in \mathbb{R}^{3 \times m}, \mathbf{H}' \in \mathbb{R}^{d \times m}$, where \mathbf{Z}, \mathbf{Z}' are coordinate transformations, while \mathbf{H}, \mathbf{H}' are feature embeddings. The core property of IEGMNs is that stacking any number of such layers guarantees that any independent rotation and translation of the original input structures will be exactly reflected in the outputs, i.e., $IEGMN(\mathbf{U}\mathbf{X} + \mathbf{b}, \mathbf{F}, \mathbf{U}'\mathbf{X}' + \mathbf{b}', \mathbf{F}') = \mathbf{U}\mathbf{Z} + \mathbf{b}, \mathbf{H}, \mathbf{U}'\mathbf{Z}' + \mathbf{b}', \mathbf{H}'$ for any orthogonal matrices $\mathbf{U}, \mathbf{U}' \in \mathbf{SO}(3)$ and translation vectors $\mathbf{b}, \mathbf{b}' \in \mathbb{R}^3$. In practice, the $\mathbf{Z}, \mathbf{H}, \mathbf{Z}', \mathbf{H}'$ outputs shown in Figure 2 are obtained by stacking several IEGMN layers. Our choice for a single l -th layer is:

$$\mathbf{m}_{j \rightarrow i} = \varphi^e(\mathbf{h}_i^{(l)}, \mathbf{h}_j^{(l)}, \|\mathbf{x}_i^{(l)} - \mathbf{x}_j^{(l)}\|^2, \mathbf{f}_{j \rightarrow i}), \forall (i, j) \in \mathcal{E} \cup \mathcal{E}'$$

$$\mu_{j' \rightarrow i} = a_{j' \rightarrow i} \mathbf{W} \mathbf{h}_{j'}^{(l)}, \forall i \in \mathcal{V}, j' \in \mathcal{V}' \text{ or } i \in \mathcal{V}', j' \in \mathcal{V}$$

$$\mathbf{m}_i = \frac{1}{|\mathcal{N}(i)|} \sum_{j \in \mathcal{N}(i)} \mathbf{m}_{j \rightarrow i}, \forall i \in \mathcal{V} \cup \mathcal{V}'$$

$$\mu_i = \sum_{j' \in \mathcal{V}'} \mu_{j' \rightarrow i}, \forall i \in \mathcal{V}, \quad \text{and} \quad \mu'_i = \sum_{j \in \mathcal{V}} \mu_{j \rightarrow i}, \forall i \in \mathcal{V}'$$

$$\mathbf{x}_i^{(l+1)} = \Psi \left(\mathbf{x}_i^{(l)} + \sum_{j \in \mathcal{N}(i)} \frac{\mathbf{x}_i^{(l)} - \mathbf{x}_j^{(l)}}{\|\mathbf{x}_i^{(l)} - \mathbf{x}_j^{(l)}\|} \varphi^x(\mathbf{m}_{j \rightarrow i}) \right)$$

$$\mathbf{h}_i^{(l+1)} = (1 - \beta) \cdot \mathbf{h}_i^{(l)} + \beta \cdot \varphi^h(\mathbf{h}_i^{(l)}, \mathbf{m}_i, \mu_i, \mathbf{f}_i), \forall i \in \mathcal{V} \cup \mathcal{V}'$$

where $a_{j \rightarrow i}$ are SE(3)-invariant attention coefficients derived from \mathbf{H} embeddings, $\mathcal{N}(i)$ are the graph neighbors of node i , \mathbf{W} is a parameter matrix, and the various φ functions are modeled using shallow neural networks, with φ^x outputting a scalar and others a d -dimensional vector.

When modeling ligand flexibility, we found it useful to incorporate additional geometric constraints on transformed coordinates through Ψ models described in Section 3.2.1.

The role of \mathbf{Z} . The output of the coordinate E(3)-equivariant transformations denoted as \mathbf{Z} and \mathbf{Z}' will be used in different roles: to identify the rigid body transformation and the binding site, as well as to model ligand flexibility by training \mathbf{Z} to represent the deformed atomic point cloud. We detail both steps below.

3.1. Rigid transformation through binding keypoints

To identify the rigid SE(3) transformation to dock the ligand in the right position and orientation, we follow (Ganea et al., 2021a) and compute ligand and receptor keypoints of size K using an SE(3)-equivariant multi-head attention mechanism defined as $\mathbf{y}_k := \sum_{i=1}^n \alpha_i^k \mathbf{z}_i$, $\mathbf{y}'_k := \sum_{j=1}^m \beta_j^k \mathbf{z}'_j$ where $\alpha_i^k = \text{softmax}_i(\frac{1}{\sqrt{d}} \mathbf{h}_{1i}^\top \mathbf{U} \mu(\varphi(\mathbf{H}_2)))$ and similarly defined β_j^k are attention coefficients, with \mathbf{U} a parametric learnable matrix. These keypoints are trained to match the ground truth binding pocket points using an optimal transport loss that recovers their alignment (detailed in (Ganea et al., 2021a)). In our case, ground truth binding pocket points are defined as midpoints of segments connecting ligand atoms to receptor atoms (e.g., from side-chains) that are closer than 4 Å. For models incorporating ligand flexibility, these pocket points are defined as all ligand atoms that are closer than 4 Å to any receptor atom. When the ligand and receptor are separated, we seek to identify the corresponding binding sites, and their exact matching using the two predicted keypoint sets $\mathbf{Y}, \mathbf{Y}' \in \mathbb{R}^{3 \times K}$. If predicted

perfectly, the SE(3) transformation to superimpose \mathbf{Y} and \mathbf{Y}' would precisely correspond to the binding SE(3) transformation to perform ligand docking and reveal the bound ligand orientation.

3.2. Modeling Chemically Plausible Ligand Flexibility

It has previously been assumed that the most flexible parts of drug-like molecules are rotatable bonds, while *local atomic structures (LAS)* (bond lengths and adjacent bond angles) or small rings are mostly rigid (Trott & Olson, 2010; Zsoldos et al., 2007; Huang, 2018; Méndez-Lucio et al., 2021). We here follow this hypothesis in two different ways as below.

We model ligand flexibility through \mathbf{Z} , which will represent a good approximation of the deformed atomic point cloud of the original conformer (i.e., into its bound structure). We train our model with two extra loss function terms: ligand-RMSD (Root-mean-square deviation) and Kabsch-RMSD¹.

3.2.1. DISTANCE GEOMETRIC CONSTRAINTS

Our first goal is to enforce LAS distance constraints in the IEGMN layers after each coordinate transformation, i.e., through a tailored differentiable function Ψ , which we call "*LAS distance geometry (DG) projection*." While a hard constraint might be difficult to impose exactly, we find the following soft strategy to work well. Formally, the transformed coordinates \mathbf{Z} satisfy the LAS DG constraints iff the following function is minimized w.r.t. \mathbf{Z} for a fixed given (random low-energy unbound) conformer \mathbf{X} :

$$\begin{aligned} \mathcal{S}(\mathbf{Z}, \mathbf{X}) = & \sum_{\{(i,j)\} \in \mathcal{E}} (d_{\mathbf{X}}^2(i,j) - d_{\mathbf{Z}}^2(i,j))^2 \\ & + \sum_{\{i,j: 2\text{-hops away in } \mathcal{G}\}} (d_{\mathbf{X}}^2(i,j) - d_{\mathbf{Z}}^2(i,j))^2 \end{aligned}$$

Thus, our definition of Ψ is hard-coding a fixed number (T) of gradient descent layers that aim to minimize \mathcal{S} :

$$\Psi(\mathbf{Z}) = \Psi_T \circ \dots \circ \Psi_1(\mathbf{Z}), \quad \Psi_t(\mathbf{Z}) = \mathbf{Z} - \eta \nabla_{\mathbf{Z}} \mathcal{S}(\mathbf{Z}, \mathbf{X}), \forall t$$

which is easy since gradients of \mathcal{S} have a simple closed-form expression and can be practically implemented efficiently with current DL frameworks. A similar approach can be employed for modeling various other rigid substructures such as aromatic rings. T and the correction step size η are model hyperparameters chosen as described in Appendix C.

3.2.2. FAST POINT CLOUD LIGAND FITTING

However, while helpful for model training, the previous gradient descent-based projection is not guaranteed to enforce hard LAS DG constraints and, thus, might produce implausible conformers in practice as we show in Figure 5.

To address this issue, we only change the torsion angles of the initial (RDKit) unbound conformer \mathbf{X} to match \mathbf{Z} as well as possible while keeping LAS fixed and, thus, hard-guaranteeing chemically plausible output bound conformers. The output will be a new conformer $\mathbf{C} \in \mathbb{R}^{3xn}$ with $\mathcal{S}(\mathbf{C}, \mathbf{X}) = 0$. First, \mathbf{C} is initialized as \mathbf{X} , and only its rotatable bonds' torsion angles are changed.

A choice is to optimize \mathbf{C} for minimizing Kabsch-RMSD(\mathbf{Z}, \mathbf{C}). However, such an approach requires an iterative optimization strategy of all torsion angles of rotatable bonds which can be done using a differential evolution algorithm as in Méndez-Lucio et al. (2021), or other local random search strategies. This is computationally expensive (e.g., 51 minutes for a single 44 rotatable bond molecule) and might fail to find a good local minimum. A gradient-based method that could better capture the various molecular interactions, but computing the gradients of a point cloud w.r.t. its bonds' torsion angles is non-trivial given the geometric dependencies between dihedral angles, i.e., Equation (2).

We present a much cheaper alternative for which a closed form solution exists (does not require optimization): we compute the dihedral angles of rotatable bonds of \mathbf{C} as maximum likelihood estimates of von Mises distributions on dihedral angles of \mathbf{Z} . Formally, this reduces to the following maximization:

$$\max_{\{\angle(kij, ijl)\}} \sum_{(k,i),(i,j),(j,l) \in \mathcal{E}} \cos(\angle_{\mathbf{Z}}(kij, ijl) - \angle(kij, ijl)) \quad (1)$$

where $\angle_{\mathbf{Z}}(kij, ijl)$ are the dihedral angles² of \mathbf{Z} , and $\angle(kij, ijl)$ are the dihedrals of \mathbf{C} that we seek to optimize.

However, we have to explicitly take into account that *all the dihedral angles for the same rotatable bond (i,j) are coupled* by the following constraint (Ganea et al., 2021b):

$$\begin{aligned} \angle(kij, ijl) = &_{2\pi} \angle(k'ij, ijl') + \angle(kij, k'ij) + \angle(ijl', ijl), \\ \forall (i,j) \in \mathcal{E}, \forall k, k' \in \mathcal{N}_i, \forall l, l' \in \mathcal{N}_j \end{aligned} \quad (2)$$

where $\angle(kij, k'ij)$ and $\angle(ijl', ijl)$ depend only on the local structures of nodes i and j , respectively, thus will not change if the torsion angle of bond (i,j) changes.

To minimize Equation (1), we can simply do it independently per each rotatable bond $(i,j) \in \mathcal{E}$. Let us fix one such bond (i,j) and use the notations: $\Delta_{kl} = \angle(kij, ijl)$ and $\beta_{kk'l'l} = \angle(kij, k'ij) + \angle(ijl', ijl)$. Additionally, for any angle α , we define: $\mathbf{A}_{\alpha} := \begin{bmatrix} \cos(\alpha) & -\sin(\alpha) \\ \sin(\alpha) & \cos(\alpha) \end{bmatrix}$ and $\mathbf{s}_{\alpha} := \begin{bmatrix} \cos(\alpha) \\ \sin(\alpha) \end{bmatrix}$. Thus, we rewrite the constraint in Equa-

¹RMSD after superimposition, or RMSD of atomic positions.

²We use clockwise angles following the chemistry convention.

275 tion (2) as $\mathbf{s}_{\Delta_{kl}} = \mathbf{A}_{\beta_{kk'l'l}} \mathbf{s}_{\Delta_{k'l'}}$, $\forall k, k' \in \mathcal{N}_i, \forall l, l' \in \mathcal{N}_j$.
 276 Equation (1) is then rewritten for bond (i,j), up to a constant:

$$\max_{\{\Delta_{kl}\}} \sum_{k \in \mathcal{N}_i} \sum_{l \in \mathcal{N}_j} \langle \mathbf{s}_{\Delta_{kl}}, \mathbf{s}_{\Delta_{kl}}^* \rangle \quad (3)$$

281 Choosing any fixed $k_0 \in \mathcal{N}_i, l_0 \in \mathcal{N}_j$, the above becomes
 282

$$\max_{\Delta_{k_0 l_0}} \sum_{k \in \mathcal{N}_i} \sum_{l \in \mathcal{N}_j} \langle \mathbf{A}_{\beta_{kk_0 l_0}} \mathbf{s}_{\Delta_{k_0 l_0}}, \mathbf{s}_{\Delta_{k_0 l_0}}^* \rangle = \mathbf{s}_{\Delta_{k_0 l_0}}^\top \mathbf{v} \quad (4)$$

286 where $\mathbf{v} := \sum_{k \in \mathcal{N}_i} \sum_{l \in \mathcal{N}_j} \mathbf{A}_{\beta_{kk_0 l_0}}^\top \mathbf{s}_{\Delta_{k_0 l_0}}^*$. This has the
 287 closed form solution $\mathbf{s}_{\Delta_{k_0 l_0}} = \frac{\mathbf{v}}{\|\mathbf{v}\|}$, which finally gives all
 288 dihedral angles Δ_{kl} in closed form. One can easily verify
 289 that the choice of $k_0 \in \mathcal{N}_i$ and $l_0 \in \mathcal{N}_j$ will not affect the
 290 values of the predicted dihedrals $\Delta_{kl}, \forall k \in \mathcal{N}_i, \forall l \in \mathcal{N}_j$.

291 In a practical example, the above solution recovers all 44
 292 rotatable bond torsion angles of a randomly modified con-
 293 former in 0.04 seconds as opposed to 3143 seconds needed
 294 by a differential evolution method.

4. Experiments

4.1. Data

300 We provide a new time-based dataset split and preprocessing
 301 pipeline for DL drug binding methods³. We use protein-
 302 ligand complexes from PDBBind (Liu et al., 2017), which
 303 is a subset of the Protein Data Bank (PDB) (Berman et al.,
 304 2003) that provides 3D structures of individual proteins and
 305 complexes. The newest version, PDBBind v2020, contains
 306 19 443 protein-ligand complexes with 3890 unique recep-
 307 tors and 15 193 unique ligands. Histograms for individual
 308 receptor and ligand data frequencies are in Figure 9 and
 309 we describe our preprocessing to remove pathologies of the
 310 data in Appendix B.

312 **Motivation for new test set and time split.** Docking meth-
 313 ods are often evaluated using the PDBBind core set, which
 314 contains 285 hand-curated high-resolution complexes. How-
 315 ever, this might not reflect the performance in real-world
 316 applications where data might not be of similar high quality.
 317 Due to the differences in resolution and the average ligand
 318 size (32 heavy atoms in PDBBind versus 24 in the core set),
 319 the complexes of the core set can be considered easier to
 320 predict than the average complex. Moreover, some of the
 321 previous methods might have been validated or trained on
 322 a subset of the core set and thus, report optimistic quality
 323 numbers. To better reflect the average complex encountered
 324 in applications, we employ a test set that only contains com-
 325 plexes that were discovered in 2019 or later, while the train
 326 and validation sets only use strictly older complexes.

327 ³We make this data and associated scripts available at <https://anonymous.4open.science/r/EquiBind-9275>.

Dataset split. Of the 19 119 preprocessed complexes, 1512 were discovered in 2019 or later. From these, we randomly sample 125 unique proteins and collect all new complexes containing them (363) to create the final test set. The low number of test samples is chosen to make it feasible to compare with time-consuming classical physics-based docking methods. From the remaining complexes that are older than 2019, we remove those with ligands contained in the test set, giving 17 347 complexes for training and validation. These are divided into 968 validation complexes, which share no ligands with the remaining 16 379 training complexes.

4.2. Evaluation Setup

Baselines. QVina-W is a classical docking program specifically developed for "wide" or blind docking. SMINA (Koes et al., 2013) builds on AutoDock Vina (Vina) by designing an improved and empirical scoring function. GNINA (McNutt et al., 2021; Francoeur et al., 2020) further develops a DL scoring function using CNNs and a grid-based featurization scheme. We run GNINA and SMINA with their default settings and for QVina-W we increase the exhaustiveness (parameter controlling the search time) to 64 since this is still computationally reasonable.

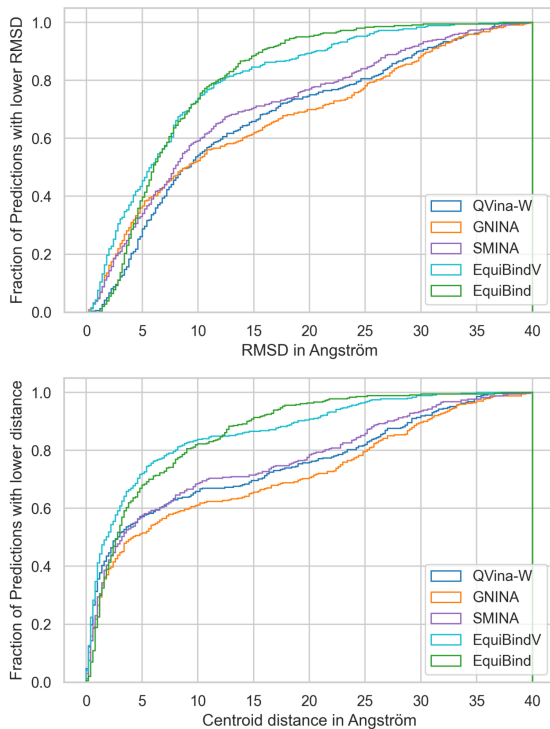
EQUIBind models. Our model can be applied in various scenarios, see caption of Table 1. First, the EQUIBIND-U model generates an uncorrected ligand that does not necessarily have realistic bond angles and lengths via the geometry constrained point cloud evolution explained in Section 3.2.1. The standard EQUIBIND takes this output and applies our fast point cloud ligand fitting in Section 3.2.2 to obtain a realistic molecular structure. The model EQUIBIND-R treats the ligand as a rigid body, being trained with no flexibility loss terms. The fine-tuning model EQUIBINDQ builds on top of this output by searching refined conformations using Quick Vina 2 in a 5 Å bounding box around the ligand predicted by EQUIBIND-R. The instantiations EQUIBINDQ+ does the same with two times as many sampled ligand positions, and EQUIBINDV instead uses Vina for fine-tuning.

Evaluation Metrics. Several metrics quantify the successful generation of a bound pose in a target, but we focus on the ligand root mean square deviation (L-RMSD) of atomic positions, the centroid distance, and the Kabsch-RMSD. The centroid distance measures the ability of the model to find the correct binding pocket (for a given ligand) by computing the distance between the centroids of the predicted and true bound ligand atoms. The Kabsch RMSD (i.e., RMSD after superimposition with the Kabsch algorithm) measures the quality of the resulting ligand conformation (distance to the bound conformer) independently on the rigid SE(3) docking transformation. L-RMSD measures the mean squared error between the atoms of the predicted and bound ligands. For each success criteria, we show cumulative distributions (e.g.,

330
 331 **Table 1. Flexible blind self-docking.** All methods receive a random RDKit conformer of the ligand molecule as input and are tasked to
 332 find the binding site and to dock it to the right orientation and in the correct conformation. EQUIBIND-U refers to the model producing
 333 uncorrected atomic point clouds \mathbf{Z} that are not necessarily chemically plausible ligands. EQUIBIND performs our fast conformer fitting
 334 corrections – see Section 3.2.2. EQUIBINDQ first predicts the ligand position while treating it as a rigid body and fine-tunes it using
 335 QuickVina 2. EQUIBINDQ+ samples more candidate positions, and EQUIBINDV uses Vina for fine-tuning.

METHODS	% AVG. CPU MIN.	LIGAND RMSD ↓						CENTROID DISTANCE ↓						KABSCH	
		PERCENTILES ↓			% BELOW THRESHOLD ↑			PERCENTILES ↓			% BELOW THRESHOLD ↑			RMSD ↓	
		MEAN	25TH	50TH	75TH	5 Å	2 Å	MEAN	25TH	50TH	75TH	5 Å	2 Å	MEAN	MEDIAN
QVINA-W	10	14.9	5.	9.8	23.5	25.0	4.7	11.72	0.8	3.5	22.5	54.7	41.6	3.8	3.7
GNINA	57	15.6	3.6	10.3	26.0	33.8	12.7	13.5	1.2	5.8	25.1	48.2	34.9	2.6	2.1
SMINA	51	13.8	4.0	8.5	21.4	31.3	11.6	11.4	1.1	3.8	20.4	54.0	38.5	2.6	2.1
EQUIBINDQ	1.3	8.9	3.3	7.0	11.8	35.5	13.3	5.8	0.92	2.43	6.4	68.7	44.9	2.6	2.2
EQUIBINDQ+	2.7	8.9	3.1	6.9	11.4	38.5	16.6	6.0	0.8	2.3	6.5	70.1	44.0	2.5	2.1
EQUIBINDV	51	8.5	2.6	5.8	10.7	43.1	19.4	5.8	0.7	2.0	5.9	71.1	49.7	2.5	2.1
EQUIBIND	0.1	8.3	3.9	6.1	10.4	38.0	3.8	5.7	1.2	2.9	7.9	66.4	38.6	2.6	2.4
EQUIBIND-U	0.1	7.8	3.2	5.7	10.2	42.7	5.5	5.7	1.2	2.9	7.9	66.4	38.6	2.2	1.8

347 25th L-RMSD refers to the L-RMSD value under which
 348 25% of the predictions fall). Finally, we report the percent
 349 of predictions below a given threshold for both metrics.



375 **Figure 3. Flexible blind self-docking.** Cumulative density histogram of the RMSD (top) and centroid distance (bottom) of
 376 EQUIBIND with and without Vina for fine-tuning.

377 **Implementation Details.** We optimize our model using
 378 Adam (Kingma & Ba, 2014) and do early stopping with
 379 patience of 150 epochs based on the percentage of predicted
 380 validation set complexes with an RMSD better than 2 Å.
 381 All hyperparameters and the employed ligand and node
 382

383 features are described in Appendix C. Code to reproduce
 384 results or perform fast docking with the provided model
 385 weights is available at <https://anonymous.4open.science/r/EquiBind-9275>.

4.3. Results

Blind self-docking. This set of experiments reflects the performance that can be expected in the most typical applications where the true ligand bond angles and distances (which are used in re-docking) are unknown. An initial approximate conformer has to be obtained from a 2D molecular graph for which we use a random RDKit conformer.

The results in Table 1 show that vanilla EQUIBIND performs well at identifying the approximate binding location and outperforms the baselines in metrics other than the 25th RMSD percentile and the fraction of predictions with and RMSD better than 2 Å. The fine-tuning extensions of EQUIBIND such as EQUIBINDQ outperform or match the baselines in all metrics, while EQUIBINDQ and EQUIBINDQ+ also retain significant inference speed-ups, making our method *suitable for extremely high-throughput applications such as virtual screening over databases of hundred million molecules, e.g., ZINC*. Thus, practitioners can combine our method with previous fine-tuning baselines and trade quality over runtime depending on the downstream task of interest.

Figure 3 shows the same trend for the RMSD. The standard EQUIBIND, which is two orders of magnitude faster than the fastest baseline, improves over the baselines for the predictions in the $> 4 \text{ \AA}$ regime. EQUIBIND does better for complexes that are hard to predict (e.g., due to ligand size) and also outperforms the baselines in the low RMSD regime when using fine-tuning (EQUIBINDV). For the **centroid distances**, the exact conformer is less crucial, and the methods mainly have to find the correct binding pocket location. Here, EQUIBIND is already able to match the baselines in

Table 2. Blind re-docking. All methods receive the ligand with the conformation as in the bound state as input and are tasked to find the binding site and to dock it to the right location and orientation. Note that EQUIBIND-R's Kabsch RMSD is 0 since it treats the ligand as a rigid body while the other methods can only be run in a flexible mode, i.e., they change torsion angles of rotatable bonds.

METHODS	% AVG. CPU	LIGAND RMSD ↓						CENTROID DISTANCE ↓						KABSCH	
		PERCENTILES ↓				% BELOW THRESHOLD ↑		PERCENTILES ↓				% BELOW THRESHOLD ↑		RMSD ↓	
		MEAN	25TH	50TH	75TH	5 Å	2 Å	MEAN	25TH	50TH	75TH	5 Å	2 Å	MEAN	MEDIAN
QVINA-W	10	13.3	1.8	7.6	23.9	38.7	26.5	11.4	0.6	3.2	22.3	57.3	43.5	2.0	1.6
GNINA	57	13.6	1.7	7.7	24.8	40.7	28.2	11.7	0.5	2.54	23.7	56.7	47.3	2.2	1.7
SMINA	51	13.0	2.4	7.9	20.9	37.1	23.8	10.7	0.5	3.3	19.7	57.6	42.6	2.1	1.6
EQUIBIND-R	0.1	7.4	2.03	5.15	9.9	48.8	25.1	5.7	1.2	2.5	7.3	66.9	40.8	0	0

the low error regime without fine-tuning. Histograms for EQUIBINDQ and EQUIBINDQ+ are in Appendix Figure 6.

The **main observations** are that EQUIBIND is much faster than the baselines, has fewer predictions that are far off from the true conformer, and can use fast fine-tuning for very low-RMSD final predictions. The benefits through fine-tuning can be expected considering the difficulty of predicting the correct torsions jointly with the binding location and orientation in a single forward pass. Visualizations of qualitative results are in Appendix Figure 4.

Blind re-docking. In these experiments, the bound ligand is extracted from the binding pocket placed in a random location, and the methods have to re-dock it into the correct conformation. Thus the methods have access to the ground truth structure of the ligand, and all predictions will have the correct bond lengths and angles. EQUIBIND-R treats the ligand as a completely rigid body and only predicts a translation and rotation since flexibility is not required in this scenario. Rigid re-docking results are of practical relevance for docking strategies where large amounts of conformations are generated for a single molecule and then rigidly docked to the receptor before using an additional scoring function to rank the predictions.

In Table 2 we can observe that EQUIBIND-R can be particularly impactful for this strategy due to its much faster inference time. This is while outperforming the baselines in the metrics other than the 25th percentiles and the fraction of predictions with an error below 2 Å. For practical rigid redocking applications, this could potentially be remedied by docking 10 times as many conformers while still retaining a 10 times speed-up over the fastest baseline.

Visualizations. EQUIBIND’s predictions are rarely far off from the true ligand, but there are cases where it struggles to find the exact atom configurations. Examples of this are in Figure 4 and show two cases where GNINA performs worse and produces a prediction that is far off while EQUIBIND is able to find the binding location. The other two cases, where GNINA is better, display how the baseline more exactly finds the true structure, but EQUIBIND still finds the correct approximate location.

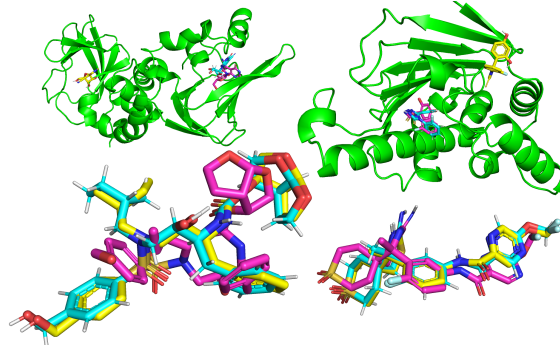


Figure 4. Two cherry-picked example predictions where EQUIBIND has better RMSD than GNINA (top) and two where EQUIBIND performs worse than GNINA (bottom). The ground truth ligand is in cyan, EQUIBIND in pink, and GNINA in yellow.

Limitations. One drawback of EQUIBIND is that it only implicitly models the atom positions of side chains. This is done via the local frame encoding features of Jumper et al. (2021a) that we employ in the α -carbon graph of the receptor. Explicitly representing these atoms might improve precise docking. We experimented with surface atoms and fine-tuning approaches that use an atom subgraph of the receptor with results in Appendix A. However, this yielded only small or no improvements while adding considerable computational complexity. We leave further exploration of this strategy for future work. These results are in line with prior protein modeling techniques such as AlphaFold2 (Jumper et al., 2021a) which successfully predicts side chains based on residue level information.

5. Conclusion

The promising ability of deep neural networks to predict protein structures has sparked a large amount of research in computational drug discovery. Here, we proposed EquiDock, a deep neural model which relies on SE(3)-equivariant graph neural networks to predict bound protein-ligand conformations in a single shot. Our model shows strong empirical performance against state-of-the-art baselines, and we demonstrate its potential in a hybrid workflow by combining it with existing fine-tuning methods.

References

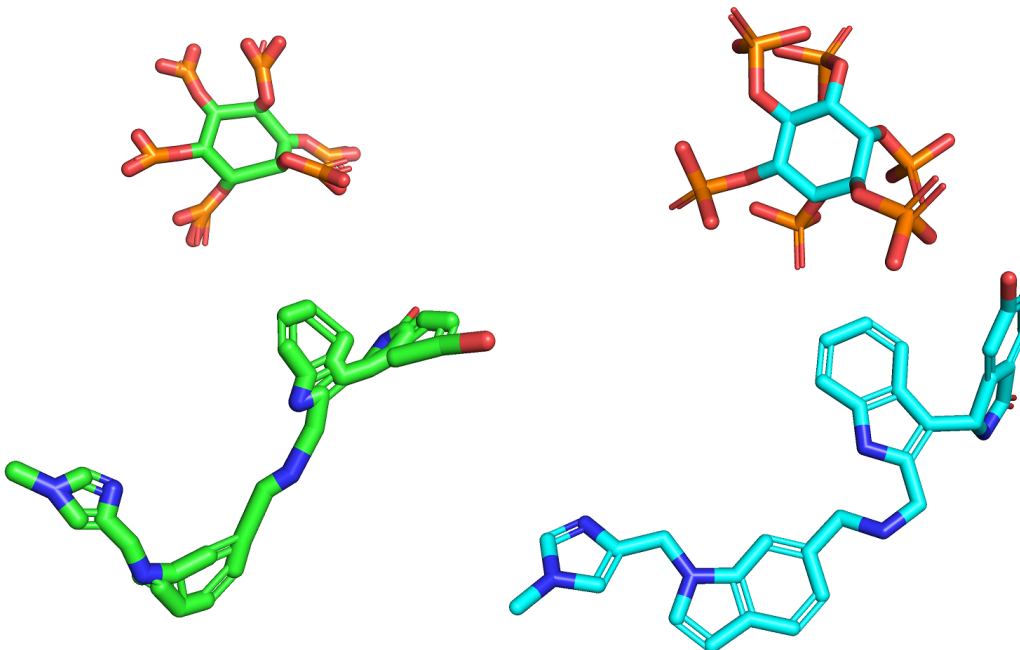
- Aggarwal, R., Gupta, A., Chelur, V., Jawahar, C., and Priyakumar, U. Deeppocket: Ligand binding site detection and segmentation using 3d convolutional neural networks, 2021.
- Baek, M., DiMaio, F., Anishchenko, I., Dauparas, J., Ovchinnikov, S., Lee, G. R., Wang, J., Cong, Q., Kinch, L. N., Schaeffer, R. D., et al. Accurate prediction of protein structures and interactions using a three-track neural network. *Science*, 373(6557):871–876, 2021.
- Bao, J., He, X., and Zhang, J. Z. Deepbsp—a machine learning method for accurate prediction of protein–ligand docking structures. *Journal of Chemical Information and Modeling*, 2021.
- Batzner, S., Musaelian, A., Sun, L., Geiger, M., Mailoa, J. P., Kornbluth, M., Molinari, N., Smidt, T. E., and Kozinsky, B. Se (3)-equivariant graph neural networks for data-efficient and accurate interatomic potentials. *arXiv preprint arXiv:2101.03164*, 2021.
- Berman, H., Henrick, K., and Nakamura, H. Announcing the worldwide Protein Data Bank. *Nat Struct Biol*, 10(12):980, Dec 2003.
- Brandstetter, J., Hesselink, R., van der Pol, E., Bekkers, E., and Welling, M. Geometric and physical quantities improve e (3) equivariant message passing. *arXiv preprint arXiv:2110.02905*, 2021.
- Cohen, T. and Welling, M. Group equivariant convolutional networks. In *International conference on machine learning*, pp. 2990–2999. PMLR, 2016.
- Dai, B. and Bailey-Kellogg, C. Protein interaction interface region prediction by geometric deep learning. *Bioinformatics*, 2021.
- de Freitas, R. F. and Schapira, M. A systematic analysis of atomic protein–ligand interactions in the pdb. *MedChemComm*, 8(10):1970–1981, 2017.
- Drotár, P., Jamasb, A. R., Day, B., Cangea, C., and Liò, P. Structure-aware generation of drug-like molecules. *arXiv preprint arXiv:2111.04107*, 2021.
- Du, X., Li, Y., Xia, Y.-L., Ai, S.-M., Liang, J., Sang, P., Ji, X.-L., and Liu, S.-Q. Insights into protein–ligand interactions: mechanisms, models, and methods. *International journal of molecular sciences*, 17(2):144, 2016.
- Eismann, S., Townshend, R. J., Thomas, N., Jagota, M., Jing, B., and Dror, R. O. Hierarchical, rotation-equivariant neural networks to select structural models of protein complexes. *Proteins: Structure, Function, and Bioinformatics*, 2020.
- Evans, R., O’Neill, M., Pritzel, A., Antropova, N., Senior, A. W., Green, T., Žídek, A., Bates, R., Blackwell, S., Yim, J., Ronneberger, O., Bodenstein, S., Zielinski, M., Bridgland, A., Potapenko, A., Cowie, A., Tunyasuvunakool, K., Jain, R., Clancy, E., Kohli, P., Jumper, J., and Hassabis, D. Protein complex prediction with alphafold-multimer. *bioRxiv*, 2021. doi: 10.1101/2021.10.04.463034.
- Francoeur, P. G., Masuda, T., Sunseri, J., Jia, A., Iovanisci, R. B., Snyder, I., and Koes, D. R. Three-dimensional convolutional neural networks and a cross-docked data set for structure-based drug design. *Journal of Chemical Information and Modeling*, 60(9):4200–4215, 2020.
- Fuchs, F. B., Worrall, D. E., Fischer, V., and Welling, M. Se(3)-transformers: 3d roto-translation equivariant attention networks. *arXiv preprint arXiv:2006.10503*, 2020.
- Gainza, P., Svärrisson, F., Monti, F., Rodola, E., Boscaini, D., Bronstein, M., and Correia, B. Deciphering interaction fingerprints from protein molecular surfaces using geometric deep learning. *Nature Methods*, 17(2):184–192, 2020.
- Ganea, O.-E., Huang, X., Bunne, C., Bian, Y., Barzilay, R., Jaakkola, T., and Krause, A. Independent se(3)-equivariant models for end-to-end rigid protein docking. *arXiv preprint arXiv:2111.07786*, 2021a.
- Ganea, O.-E., Pattanaik, L., Coley, C. W., Barzilay, R., Jensen, K. F., Green, W. H., and Jaakkola, T. S. Geomol: Torsional geometric generation of molecular 3d conformer ensembles. *arXiv preprint arXiv:2106.07802*, 2021b.
- Gao, K. Y., Fokoue, A., Luo, H., Iyengar, A., Dey, S., and Zhang, P. Interpretable drug target prediction using deep neural representation. In *IJCAI*, volume 2018, pp. 3371–3377, 2018.
- Gligorijević, V., Renfrew, P. D., Kosciolék, T., Leman, J. K., Berenberg, D., Vatanen, T., Chandler, C., Taylor, B. C., Fisk, I. M., Vlamakis, H., et al. Structure-based protein function prediction using graph convolutional networks. *Nature communications*, 12(1):1–14, 2021.
- Gniewek, P., Worley, B., Stafford, K., Bedem, H. v. d., and Anderson, B. Learning physics confers pose-sensitivity in structure-based virtual screening. *arXiv preprint arXiv:2110.15459*, 2021.
- Halgren, T. A., Murphy, R. B., Friesner, R. A., Beard, H. S., Frye, L. L., Pollard, W. T., and Banks, J. L. Glide: a new approach for rapid, accurate docking and scoring. 2. enrichment factors in database screening. *Journal of medicinal chemistry*, 47(7):1750–1759, 2004.

- 495 Hassan, N. M., Alhossary, A. A., Mu, Y., and Kwoh, C.-
 496 K. Protein-ligand blind docking using quickvina-w with
 497 inter-process spatio-temporal integration. *Scientific re-*
 498 *ports*, 7(1):1–13, 2017.
- 499
- 500 Huang, S.-Y. Comprehensive assessment of flexible-ligand
 501 docking algorithms: current effectiveness and challenges.
 502 *Briefings in bioinformatics*, 19(5):982–994, 2018.
- 503 Imrie, F., Hadfield, T. E., Bradley, A. R., and Deane, C. M.
 504 Deep generative design with 3d pharmacophoric con-
 505 straints. *bioRxiv*, 2021.
- 506
- 507 Jastrzebski, S., Szymczak, M., Pocha, A., Mordalski, S.,
 508 Tabor, J., Bojarski, A. J., and Podlewska, S. Emulat-
 509 ing docking results using a deep neural network: a new
 510 perspective for virtual screening. *Journal of Chemical
 511 Information and Modeling*, 60(9):4246–4262, 2020.
- 512
- 513 Jiang, D., Hsieh, C.-Y., Wu, Z., Kang, Y., Wang, J., Wang,
 514 E., Liao, B., Shen, C., Xu, L., Wu, J., et al. Interaction-
 515 graphnet: A novel and efficient deep graph representation
 516 learning framework for accurate protein–ligand interac-
 517 tion predictions. *Journal of medicinal chemistry*, 2021.
- 518 Jiménez, J., Doerr, S., Martínez-Rosell, G., Rose, A. S., and
 519 De Fabritiis, G. Deepsite: protein-binding site predictor
 520 using 3d-convolutional neural networks. *Bioinformatics*,
 521 33(19):3036–3042, 2017.
- 522
- 523 Jindal, A., Kotelnikov, S., Padhorny, D., Kozakov, D., Zhu,
 524 Y., Chowdhury, R., and Vajda, S. Side-chain packing
 525 using se (3)-transformer. In *PACIFIC SYMPOSIUM ON
 526 BIOCOMPUTING 2022*, pp. 46–55. World Scientific,
 527 2021.
- 528
- 529 Jing, B., Eismann, S., Suriana, P., Townshend, R. J. L., and
 530 Dror, R. Learning from protein structure with geomet-
 531 ric vector perceptrons. In *International Conference on
 532 Learning Representations*, 2020.
- 533
- 534 Jumper, J., Evans, R., Pritzel, A., Green, T., Figurnov, M.,
 535 Ronneberger, O., Tunyasuvunakool, K., Bates, R., Žídek,
 536 A., Potapenko, A., Bridgland, A., Meyer, C., Kohl, S.
 537 A. A., Ballard, A. J., Cowie, A., Romera-Paredes, B.,
 538 Nikolov, S., Jain, R., Adler, J., Back, T., Petersen, S.,
 539 Reiman, D., Clancy, E., Zielinski, M., Steinegger, M.,
 540 Pacholska, M., Berghammer, T., Bodenstein, S., Silver,
 541 D., Vinyals, O., Senior, A. W., Kavukcuoglu, K., Kohli,
 542 P., and Hassabis, D. Highly accurate protein structure
 543 prediction with alphafold. *Nature*, 596(7873), Aug 2021a.
- 544
- 545 Jumper, J., Evans, R., Pritzel, A., Green, T., Figurnov, M.,
 546 Ronneberger, O., Tunyasuvunakool, K., Bates, R., Žídek,
 547 A., Potapenko, A., et al. Highly accurate protein structure
 548 prediction with alphafold. *Nature*, 596(7873):583–589,
 549 2021b.
- Karimi, M., Wu, D., Wang, Z., and Shen, Y. Deepaffinity: in-
 terpretable deep learning of compound–protein affinity
 through unified recurrent and convolutional neural
 networks. *Bioinformatics*, 35(18):3329–3338, 2019.
- Kingma, D. P. and Ba, J. Adam: A method for stochastic
 optimization. *arXiv preprint arXiv:1412.6980*, 2014.
- Koes, D. R., Baumgartner, M. P., and Camacho, C. J.
 Lessons learned in empirical scoring with smina from
 the csar 2011 benchmarking exercise. *Journal of chemi-
 cal information and modeling*, 53(8):1893–1904, 2013.
- Landrum, G. Rdkit: Open-source cheminformatics software,
 2016.
- Lang, P. T., Brozell, S. R., Mukherjee, S., Pettersen, E. F.,
 Meng, E. C., Thomas, V., Rizzo, R. C., Case, D. A.,
 James, T. L., and Kuntz, I. D. Dock 6: Combining tech-
 niques to model rna–small molecule complexes. *Rna*, 15
 (6):1219–1230, 2009.
- Li, S., Zhou, J., Xu, T., Huang, L., Wang, F., Xiong, H.,
 Huang, W., Dou, D., and Xiong, H. Structure-aware
 interactive graph neural networks for the prediction of
 protein–ligand binding affinity. In *Proceedings of the 27th
 ACM SIGKDD Conference on Knowledge Discovery &
 Data Mining*, pp. 975–985, 2021.
- Li, Y., Gu, C., Dullien, T., Vinyals, O., and Kohli, P. Graph
 matching networks for learning the similarity of graph
 structured objects. In *International Conference on Ma-
 chine Learning*, pp. 3835–3845. PMLR, 2019.
- Lim, J., Ryu, S., Park, K., Choe, Y. J., Ham, J., and Kim,
 W. Y. Predicting drug–target interaction using a novel
 graph neural network with 3d structure-embedded graph
 representation. *Journal of chemical information and mod-
 eling*, 59(9):3981–3988, 2019.
- Liu, Z., Su, M., Han, L., Liu, J., Yang, Q., Li, Y., and Wang,
 R. Forging the basis for developing protein–ligand inter-
 action scoring functions. *Accounts of Chemical Research*,
 50(2):302–309, 2017.
- Luo, S., Shi, C., Xu, M., and Tang, J. Predicting molecular
 conformation via dynamic graph score matching. *Ad-
 vances in Neural Information Processing Systems*, 34,
 2021.
- Macari, G., Toti, D., and Polticelli, F. Computational meth-
 ods and tools for binding site recognition between pro-
 teins and small molecules: from classical geometrical
 approaches to modern machine learning strategies. *Jour-
 nal of computer-aided molecular design*, 33(10):887–903,
 2019.

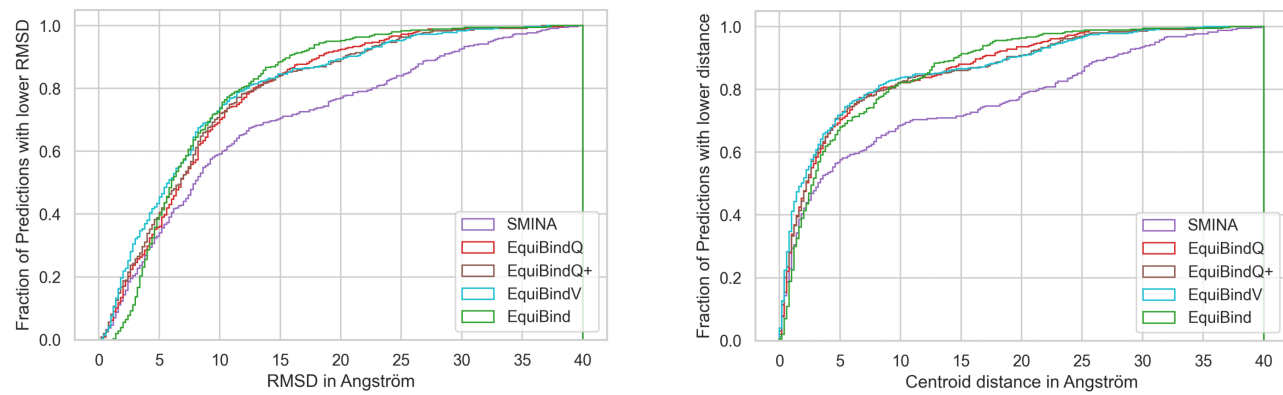
- 550 Masuda, T., Ragoza, M., and Koes, D. R. Generating
 551 3d molecular structures conditional on a receptor binding
 552 site with deep generative models. *arXiv preprint arXiv:2010.14442*, 2020.
- 553
- 554 McNutt, A. T., Francoeur, P., Aggarwal, R., Masuda, T.,
 555 Meli, R., Ragoza, M., Sunseri, J., and Koes, D. R. Gnina
 556 1.0: molecular docking with deep learning. *Journal of
 557 cheminformatics*, 13(1):1–20, 2021.
- 558
- 559 Méndez-Lucio, O., Ahmad, M., del Rio-Chanona, E. A.,
 560 and Wegner, J. K. A geometric deep learning approach
 561 to predict binding conformations of bioactive molecules.
 562 *Nature Machine Intelligence*, 3(12):1033–1039, 2021.
- 563
- 564 Mohammad, T., Mathur, Y., and Hassan, M. I. Instadock:
 565 A single-click graphical user interface for molecular
 566 docking-based virtual high-throughput screening. *Briefings
 567 in Bioinformatics*, 22(4):bbaa279, 2021.
- 568
- 569 Morrone, J. A., Weber, J. K., Huynh, T., Luo, H., and Cor-
 570 nell, W. D. Combining docking pose rank and structure
 571 with deep learning improves protein–ligand binding mode
 572 prediction over a baseline docking approach. *Journal of
 573 chemical information and modeling*, 60(9):4170–4179,
 574 2020.
- 575
- 576 Open Babel development team. Open babel, 2005. URL
 577 http://openbabel.org/wiki/Main_Page.
- 578
- 579 Ragoza, M., Hochuli, J., Idrobo, E., Sunseri, J., and Koes,
 580 D. R. Protein–ligand scoring with convolutional neural
 581 networks. *Journal of chemical information and modeling*,
 582 57(4):942–957, 2017.
- 583
- 584 Reymond, J.-L. and Awale, M. Exploring chemical space
 585 for drug discovery using the chemical universe database.
 586 *ACS chemical neuroscience*, 3(9):649–657, 2012.
- 587
- 588 Riniker, S. and Landrum, G. A. Better informed distance
 589 geometry: using what we know to improve confor-
 590 mation generation. *Journal of chemical information and
 591 modeling*, 55(12):2562–2574, 2015.
- 592
- 593 Sankararaman, S., Sha, F., Kirsch, J. F., Jordan, M. I., and
 594 Sjölander, K. Active site prediction using evolutionary
 595 and structural information. *Bioinformatics*, 26(5):617–
 596 624, 2010.
- 597
- 598 Satorras, V. G., Hoogeboom, E., and Welling, M. E(n)-
 599 equivariant graph neural networks. *arXiv preprint
 600 arXiv:2102.09844*, 2021.
- 601
- 602 Shen, C., Hu, X., Gao, J., Zhang, X., Zhong, H., Wang,
 603 Z., Xu, L., Kang, Y., Cao, D., and Hou, T. The impact
 604 of cross-docked poses on performance of machine learning
 605 classifier for protein–ligand binding pose prediction.
 606 *Journal of cheminformatics*, 13(1):1–18, 2021.
- 607
- 608 Shi, C., Luo, S., Xu, M., and Tang, J. Learning gradi-
 609 ent fields for molecular conformation generation. *arXiv
 610 preprint arXiv:2105.03902*, 2021.
- 611
- 612 Somnath, V. R., Bunne, C., and Krause, A. Multi-scale
 613 representation learning on proteins. *Advances in Neural
 614 Information Processing Systems*, 34, 2021.
- 615
- 616 Sverrisson, F., Feydy, J., Correia, B. E., and Bronstein,
 617 M. M. Fast end-to-end learning on protein surfaces. In
 618 *Proceedings of the IEEE/CVF Conference on Computer
 619 Vision and Pattern Recognition*, pp. 15272–15281, 2021.
- 620
- 621 Thomas, N., Smidt, T., Kearnes, S., Yang, L., Li, L.,
 622 Kohlhoff, K., and Riley, P. Tensor field networks:
 623 Rotation-and translation-equivariant neural networks for
 624 3d point clouds. *arXiv preprint arXiv:1802.08219*, 2018.
- 625
- 626 Torng, W. and Altman, R. B. Graph convolutional neural
 627 networks for predicting drug-target interactions. *Journal of
 628 chemical information and modeling*, 59(10):4131–4149,
 629 2019a.
- 630
- 631 Torng, W. and Altman, R. B. High precision protein func-
 632 tional site detection using 3d convolutional neural net-
 633 works. *Bioinformatics*, 35(9):1503–1512, 2019b.
- 634
- 635 Townshend, R., Bedi, R., Suriana, P., and Dror, R. End-to-
 636 end learning on 3d protein structure for interface predic-
 637 tion. *Advances in Neural Information Processing Systems*,
 638 32:15642–15651, 2019.
- 639
- 640 Trott, O. and Olson, A. J. Autodock vina: improving the
 641 speed and accuracy of docking with a new scoring func-
 642 tion, efficient optimization, and multithreading. *Journal
 643 of computational chemistry*, 31(2):455–461, 2010.
- 644
- 645 Wallach, I., Dzamba, M., and Heifets, A. Atomnet: a
 646 deep convolutional neural network for bioactivity predic-
 647 tion in structure-based drug discovery. *arXiv preprint
 648 arXiv:1510.02855*, 2015.
- 649
- 650 Xu, M., Luo, S., Bengio, Y., Peng, J., and Tang, J. Learning
 651 neural generative dynamics for molecular conformation
 652 generation. In *International Conference on Learning
 653 Representations*, 2020.
- 654
- 655 Zhang, W., Bell, E. W., Yin, M., and Zhang, Y. Edock: blind
 656 protein–ligand docking by replica-exchange monte carlo
 657 simulation. *Journal of cheminformatics*, 12:1–17, 2020.
- 658
- 659 Zsoldos, Z., Reid, D., Simon, A., Sadjad, S. B., and Johnson,
 660 A. P. ehits: a new fast, exhaustive flexible ligand docking
 661 system. *Journal of Molecular Graphics and Modelling*,
 662 26(1):198–212, 2007.

605 A. Additional Results

606
Fast point cloud fitting. In Figure 5 we visualize our novel fast point cloud ligand fitting described in Section 3.2.2. The
607 point clouds produced by the uncorrected flexible EQUIBIND-U are not realistic molecules. The corrections use a conformer
608 with valid bond lengths and angles and change its torsions to most closely match the point cloud.
609

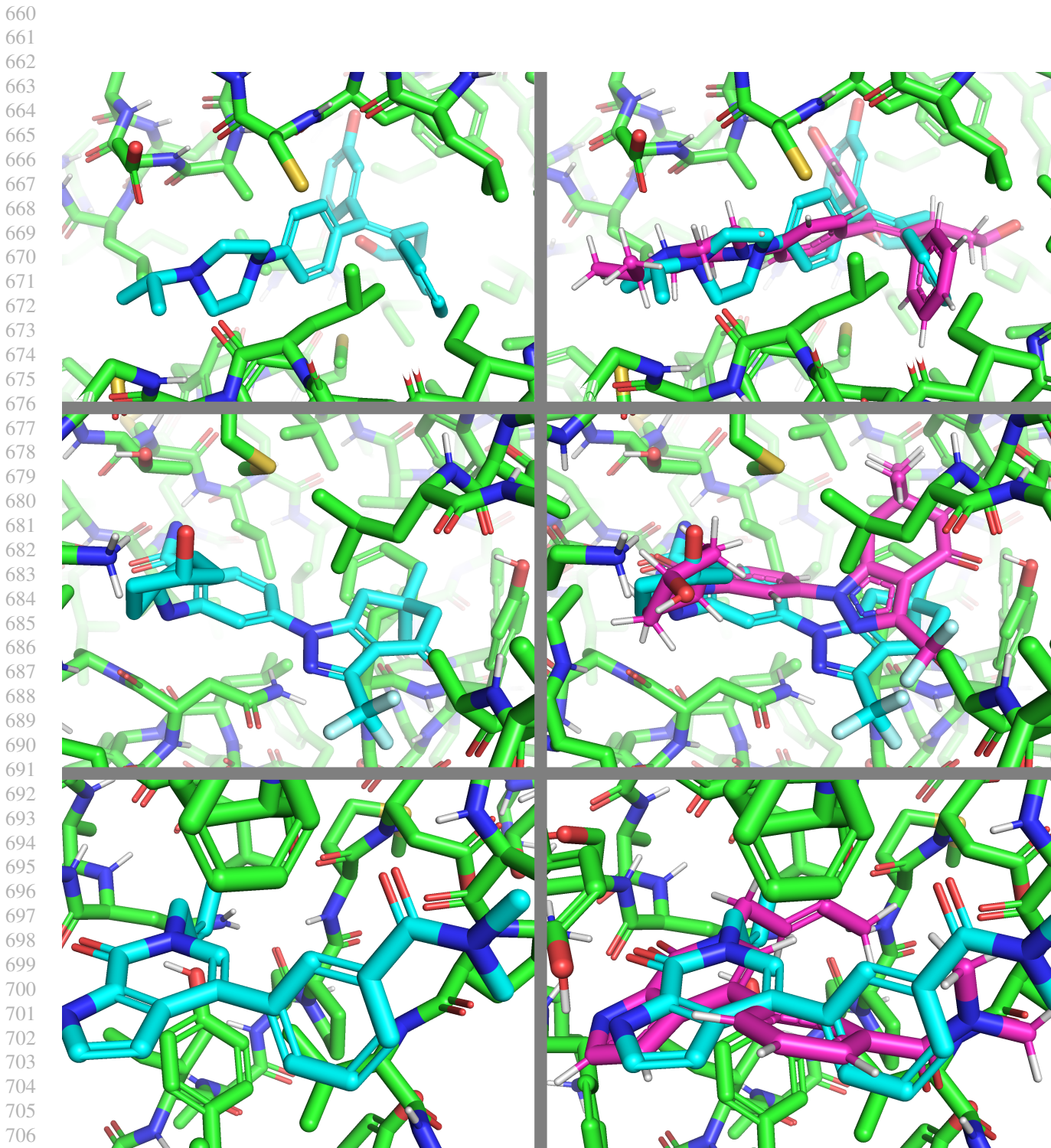


632 *Figure 5.* Left: in green are two uncorrected pseudo-molecules predicted by EQUIBIND-U. Right: the final output of EQUIBIND with
633 corrections using our fast flexible conformer fitting applied to produce a conformer with realistic bond angles and lengths.
634



650 **Figure 6. Flexible blind self-docking.** Left: Cumulative density histogram of the RMSD. Right: Cumulative density histogram of the
651 centroid distance.
652

653 In Table 3 we compare EQUIBIND which only implicitly uses atom level locations with approaches that explicitly use atoms
654 as nodes in the processed graph. EQUIBIND-S, which uses the surface atoms of the receptor, which are found using the
655 MSMS tool. EQUIBIND-A first makes a prediction using EQUIBIND-R and then uses an all-atom subgraph in a 10 Å radius
656 around the predicted ligand to further refine the prediction. This requires an additional computation step during inference
657 but does not significantly impact runtime since most of it is taken up by preprocessing. Both methods require around 2-3
658 times more GPU RAM than EQUIBIND-R.
659



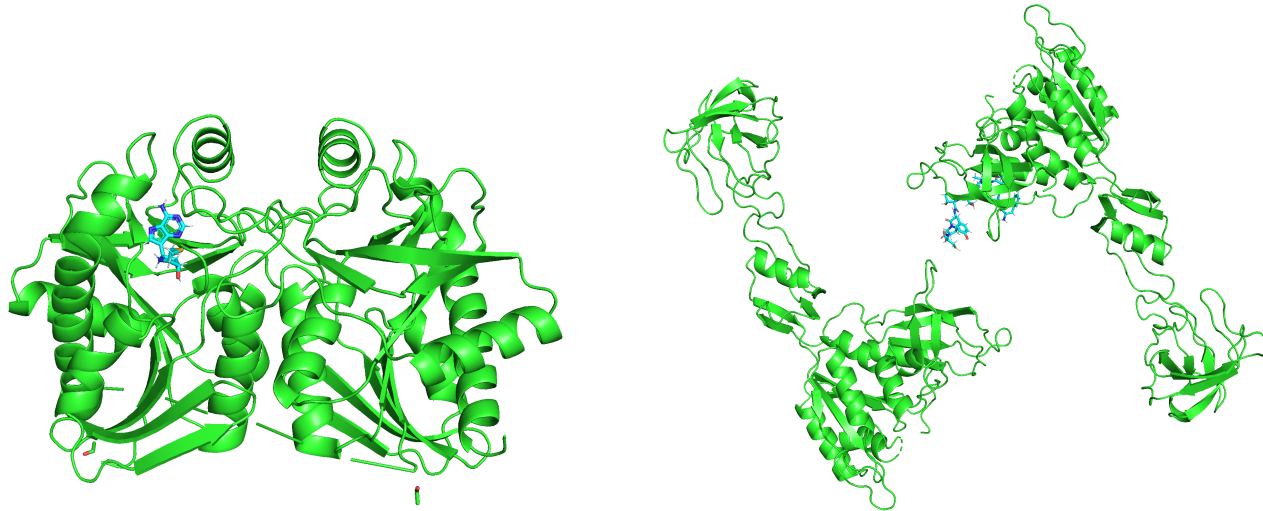
715
 716 **Table 3. Blind re-docking.** All methods receive ligand with the conformation as in the bound state as input and are tasked to find the
 717 binding site and to dock it to the right orientation and in the correct conformation. Comparison EQUIBIND with EQUIBIND-S which
 718 additionally uses the surface atoms of the receptor and EQUIBIND-A which first makes a prediction using EQUIBIND-R and then uses an
 719 all-atom subgraph in a 10 Å radius around the predicted ligand to further refine the prediction. The predictions of EQUIBIND-A have to
 720 be compared with EQUIBIND-U as it also produces unrealistic conformers. Note that Kabsch RMSDs are 0 since the ligand is treated as a
 721 rigid body.

METHODS	% AVG. CPU MIN.	LIGAND RMSD ↓						CENTROID DISTANCE ↓						KABSCH		
		PERCENTILES ↓				% BELOW THRESHOLD ↑		PERCENTILES ↓				% BELOW THRESHOLD ↑		RMSD ↓	MEAN	MEDIAN
		MEAN	25TH	50TH	75TH	5 Å	2 Å	MEAN	25TH	50TH	75TH	5 Å	2 Å	MEAN	MEDIAN	
EQUIBIND	0.1	8.3	3.9	6.1	10.4	38.0	3.8	5.7	1.2	2.9	7.9	66.4	38.6	2.6	2.4	
EQUIBIND-S	0.1	8.7	3.7	6.1	11.6	39.9	3.5	6.0	1.3	2.6	7.1	66.9	40.5	2.4	2.0	
EQUIBIND-A	0.1	8.2	3.8	6.02	10.1	42.9	3.0	6.1	1.5	3.3	7.0	62.8	31.9	3.0	2.7	
EQUIBIND-U	0.1	7.8	3.2	5.7	10.2	42.7	5.5	5.7	1.2	2.9	7.9	66.4	38.6	2.2	1.8	

B. Dataset

733 **Preprocessing.** The time split is done after preprocessing the 19 443 complexes of PDBBind v2020 as follows. First, we
 734 drop all complexes that cannot be processed by the RDKit library (Landrum, 2016), leaving 19 119 complexes. We process
 735 each ligand and receptor with OpenBabel (Open Babel development team, 2005) and add all missing hydrogens to the
 736 ligands using RDKit. Next we correct all receptor hydrogens and add missing ones using `reduce`⁴.

737 A significant remaining data issue is symmetric receptor structures comprised of the same protein repeated multiple times.
 738 In these cases, the ligand could equally likely bind to the pocket of each of the proteins, i.e., multiple ligand correct positions
 739 are possible. However, the ground truth ligand is only placed in one of those locations. Examples are in Figure 8. We
 740 address the majority of these cases by only keeping the connected components of the receptor, which have an atom within a
 741 10 Å radius of any ligand atom.



761 *Figure 8.* Examples of symmetric receptor complexes with multiple equally valid binding positions for the ligand.

C. Implementation Details

764 For the α -carbons in the receptor graph, we use the residue type as a feature. The edges have two attributes. Firstly,
 765 the interatomic distances encoded with Gaussian basis functions with 15 different variances—secondly, the local frame

766 ⁴<https://github.com/r1abduke/reduce>

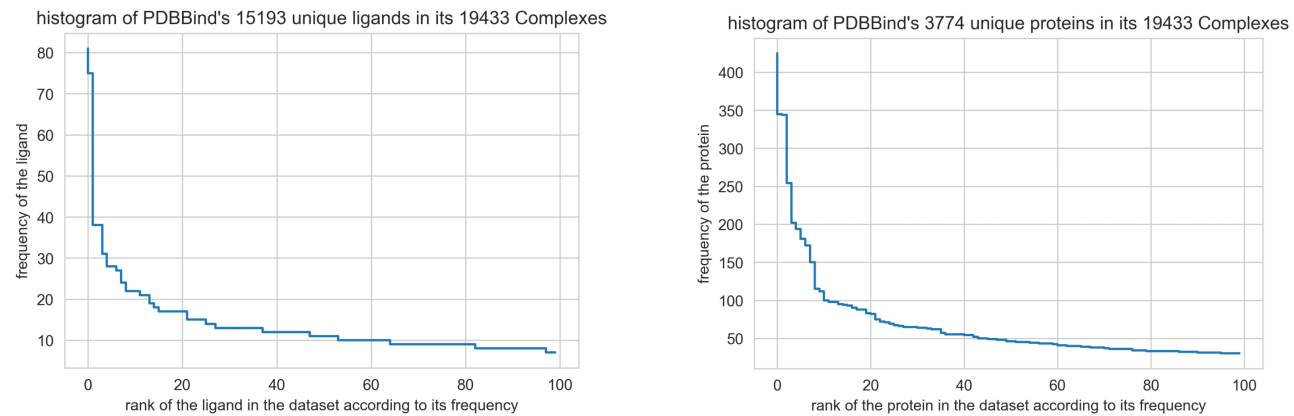


Figure 9. Histograms that show how often each unique ligand and receptor appears in the PDBBind dataset.

orientation encodings as they are employed by Jumper et al. (2021a) and (Ganea et al., 2021a).

In the ligand, the edges have features that are encoded in the same fashion as for the receptor. Meanwhile, the atoms have the following features: atomic number; chirality; degree; formal charge; implicit valence; the number of connected hydrogens; the number of radical electrons; hybridization type; whether or not it is in an aromatic ring; in how many rings it is; and finally, 6 features for whether or not it is in a ring of size 3, 4, 5, 6, 7, or 8.

We use a learning rate of 10^{-4} for EQUIBIND and 3×10^{-4} for EQUIBIND-R. The learning rate is reduced by a factor of 0.6 after 60 epochs of no improvement in our main validation criterion which is the percentage of predicted validation set complexes with an RMSD better than 2 Å. The models with the best validation score are then tested on the time-based test set.

Table 4. Search space for all EQUIBIND models through which we searched to obtain a strong performance on the validation set. The final parameters for the standard EQUIBIND model are marked in **bold**.

PARAMETER	SEARCH SPACE
LAS DG STEP SIZE η	1, 0.01, 0.001 , 0.0001
LAS DG NUMBER OF STEPS T	1, 5, 10
OPTIMAL TRANSPORT LOSS WEIGHT	0, 0.1, 0.5, 1 , 2, 10
INTERSECTION LOSS WEIGHT	0, 0.1, 1, 3 , 10, 50, 100
PROPAGATION DEPTH	[5, 7, 8]
INTERSECTION σ	8 (BASED ON LOSS ON VAL-SET)
INTERSECTION γ	8 (BASED ON LOSS ON VAL-SET)
KABSCH RMSD LOSS WEIGHT	0, 1
HIDDEN DIMENSION	32, 64 , 100
NON LINEARITIES	LEAKY-RELU , RELU, SELU
LEARNING RATES	0.0009, 0.0003, 0.0001 , 0.00007
DROPOUT	0, 0.05, 0.1 , 0.2
NUM ATTENTION HEADS	10, 20, 30 , 50, 100
NORMALIZATION	BATCHNORM , LAYERNORM, GRAPHNORM